Materials Science and Engineering B 177 (2012) 359–366

Contents lists available at SciVerse ScienceDirect

Materials Science and Engineering B

journal homepage: www.elsevier.com/locate/mseb

Influence of NiCr/Au electrodes and multilayer thickness on the electrical properties of PANI/PVS ultrathin film grown by Lbl deposition

M.C. Santos[a,b], M.L. Munford[a], R.F. Bianchi[b,*,1]

[a] Department of Physics, Federal University of Viçosa, CEP 36570-000, Viçosa, MG, Brazil
[b] Laboratory of Polymers and Electronic Properties of Materials, Department of Physics, Federal University of Ouro Preto, CEP 35400-000, Ouro Preto, MG, Brazil

ARTICLE INFO

Article history:
Received 17 August 2011
Received in revised form 8 December 2011
Accepted 23 December 2011
Available online 9 January 2012

Keywords:
Complex impedance
Semiconducting polymers
Interface
Surface
Device

ABSTRACT

In the present work, we concentrate on the study of effects of metallic electrodes, multilayer thickness and temperature in ac and dc electrical conductivity of polyaniline/poly(vinyl sulfonic acid) (PANI/PVS) ultrathin films. The polymer system was obtained from layer-by-layer (Lbl) self-assembly technique on a glass substrate with an electrode array of adhesion layer of NiCr (20 nm) covered with Au (180 nm). We observed a significant and abrupt increase in the value of dc conductivity and a change of ac conductivity behavior of NiCr/Au–PANI/PVS–NiCr/Au structure when the thickness of PANI/PVS system reaches the Au layer. These effects were ascribed to the ideal contact of Au–PANI/PVS and the relative high interfacial contact resistance between PANI/PVS and NiCr, thus reducing the parallel resistance of NiCr/Au–PANI/PVS interfacial layer in an ideal parallel plate capacitor structure. Atomic Force Microscopy images confirm this assumption. Furthermore, the ac conductivity of Au–PANI/PVS–Au structure was typical of solid disordered materials. A model based on carrier hopping in a medium with randomly varying energy barriers was presented for the ac conductivity of the polymer system, which also encompasses the high dielectric constant of PANI/PVS blended films, the neutral contact Au–PANI/PVS, and the electrical resistance of NiCr–PANI/PVS interfacial layer. The model allowed separating the interface and the bulk effects in the electrical response of NiCr/Au–PANI/PVS–NiCr/Au structure and in addition the highest activation energy (35 MeV) correlated with an optimization of hopping distance (30 nm) for carriers jumps in PANI/PVS system.

1. Introduction

A significant application growth in the area of organic semiconductors over the past few years has been well recognized by the scientific community [1–4]. The advancement is especially noticeable in the electrical response of organic electronic system such as electronic tongue, flexible chemical sensors, organic field effect transistors and thin film organic photovoltaic devices. Many applications of the organic semiconductors require the controlled assembly of polymer films as multilayer structures on solid substrates. This is the case of chemical sensors based on nanostructure polymer films prepared by layer-by-layer (Lbl) technique [5]. This technique is promising because it can lead to nanostructures similar to those built with the Langmuir–Blodgett (LB) technique [6], but yet has the advantage of requiring much simpler experimental procedures [7,8]. Among the semiconducting polymers used to fabricate Lbl films, polyaniline (PANI) appears as a potential candidate from the technological standpoint on account of its low cost and ability to behave either as a semiconductor or as a metal [9]. Meanwhile, although there are studies about the role of film thickness on the morphology [10] and electrical response [11,12] of ultrathin PANI films, an overall understanding of the charge carrier transport mechanism in PANI Lbl films has become a key to the development of devices with specific and optimized properties for organic sensors [13]. As a consequence, a detailed investigation of electrical properties of Lbl polymeric device requires the knowledge of several factors, including, for example, the influence of polymer bulk, polymer morphology and polymer–electrode interactions [14–16] in such a way that quantify the influence of these characteristics on the electrical properties of the device is important and also extremely complicated. In order to overcome these difficulties, impedance spectroscopy and complex conductivity measurements appears as a powerful tool for

* Corresponding author at: Campus Morro do Cruzeiro, CEP 35400-000, Ouro Preto, MG, Brazil. Tel.: +55 31 3559 1742; fax: +55 31 3559 1667.
E-mail addresses: bianchi@eecs.berkeley.edu, bianchi@eecs.berkeley.edu (R.F. Bianchi).
[1] Temporary address: Department of Electrical Engineering and Computer Sciences, University of California at Berkeley, 2299 Piedmont - Berkeley, CA, Brazil. Tel.: +1 510 3252126.

0921-5107/$ – see front matter © 2012 Elsevier B.V. All rights reserved.
doi:10.1016/j.mseb.2011.12.039

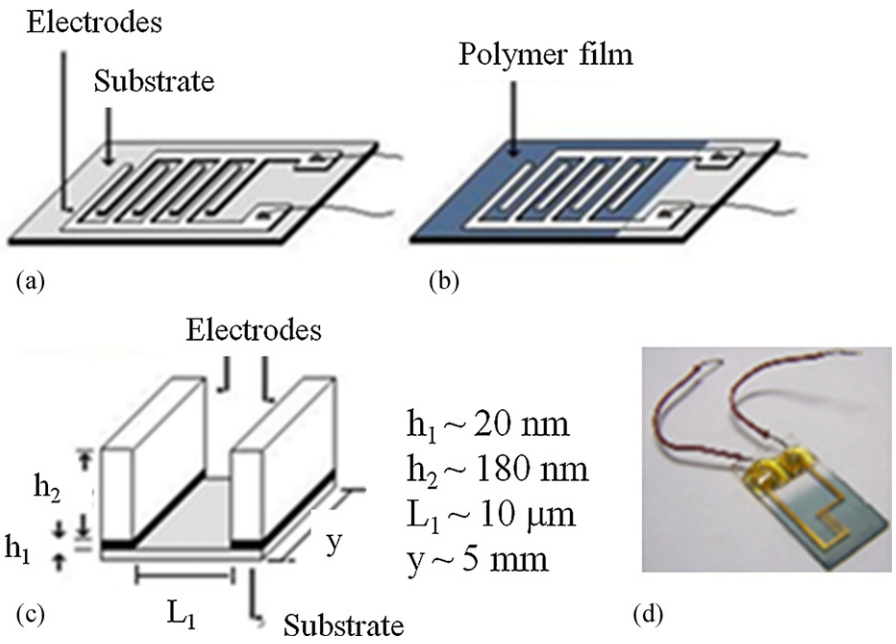

Fig. 1. Schematic illustration of (a) interdigitated microelectrodes on glass substrate. (b) PANI/PVS films onto NiCr–Au electrodes covered by polymer film. (c) Only one pair of interdigitated microelectrode with its dimensions, where its length (L_1), interdigitated spacing (y) and NiCr (h_1) and Au (h_2) thicknesses are, 5 mm, 10 μm, 20 nm and 180 nm, respectively. (d) Picture of the polymer system used to carry out the electrical measurements.

studying the electrical mechanism of organic systems, since it allows us to distinguish from bulk to interface influences, as well as to obtain polymer bulk and polymer–electrode interface contributions to electrical current [14–17]. However, in order to describe such measurements of polymer films, many authors usually represented their electrical characteristics as a circuit expression based on resistor–capacitor (RC) circuits [18,19], where both polymer layer and polymer–electrode interfaces are described by a single dielectric relaxation times, rather than a more realistic distribution expected for solid disorder materials [20]. Although in most of the case it is in good agreement with experimental data, it is not sufficient to explain – with great accuracy – the effect of carriers hopping on the polymer systems.

In this paper we investigated the dc and ac electrical behavior of films containing alternated layers of PANI and the anionic polyelectrolyte – poly(vinyl sulfonic acid) (PVS), deposited on an electrode array of adhesion layer of NiCr covered with Au (NiCr/Au), aiming at understanding the influence of film thickness and the metallic electrodes on the electrical properties of polymer bulk and metal–polymer interfacial layers. One model based on random free energy barrier model (RFEB) [21,22] is presented for the ac conductivity of the polymer system, which encompasses the disordered and dielectric properties of Lbl films, as well as the NiCr–PANI/PVS interfacial effects, which allowed separating the interface and the bulk effects in the electrical response of NiCr/Au–PANI/PVS–NiCr/Au structure.

2. Experimental procedures

PANI was synthesized according to the route described by Chiang and MacDiarmid [23] while PVS used as the polyanion was purchased from Aldrich Co. PANI was dissolved in dimethyl acetamide (DMAc) at a concentration of 10 mg/mL by stirring the solution and then was sonicated for 12 h. The solution was then filtered with a ceramic filter with 8 μm pores to remove the trace of undissolved PANI particles. Later, the PANI solution was diluted with aqueous solution 1:9 and the pH was adjusted to 3.0 by the addition of a 1 M HCl. The experimental procedures for film fabrication are essentially as described elsewhere. [7] For the building of multilayers through layer-by-layer technique, PANI was alternated with PVS, where the latter was diluted in ultrapure water, with 100 μL of a 25 wt% aqueous solution of PVS (Aldrich) being mixed with 24 mL of aqueous solution with pH 4.0. The rinsing solution was water with its pH adjusted to 2.5 with 1 M HCl. The multilayers were assembled by the alternating immersion of the substrate in the PANI and PVS solutions for 5 min each at room temperature (25 °C). After each deposition, the substrates were rinsed for 20 s in an aqueous washing solution with subsequent drying under an air flow. Films of PANI/PVS were adsorbed on BK7 optical glass. The hydrophilic substrates were obtained using the physic treatment UV–ozone cleaning. [24] The UV–ozone cleaning consisted of exposing the sample to ultraviolet radiation from a germicidal lamp in atmosphere.

The PANI/PVS adsorption was monitored by measuring the UV–vis spectra with a Spectrophotometer UV-1650PC Shimadzu. For the electrical measurements, PANI/PVS films with different number of bilayers (n) were deposited onto NiCr adhesion line array completely covered by Au [25] previously evaporated on BK7 optical glass substrates using photolithography procedure, where its length (L_1), interdigitated spacing (y) and NiCr (h_1) and Au (h_2) thicknesses provided by the manufacturer are around 10 μm, 5 mm, 20 nm and 180 nm, respectively.

Fig. 1 shows the schematic illustration of the samples. A rough estimation of a single bilayer (h) was obtained by measuring the thickness of a 40 bilayers film on BK7 substrate using a Veeco Dektak 150 Surface Profilometer. Atomic Force Microscopy (AFM) images were obtained with NTEGRA Probe NanoLaboratory. Current vs. voltage (I vs. V) measurements were obtained with a 6517A Electrometer High/Resistance Meter Keithley in the −1 V to 1 V voltage range, while complex impedance, $Z^*(f) = Z'(f) + iZ''(f)$, and thus alternating conductivity, $\sigma^*(f) = \sigma'(f) + i\sigma''(f) = (L_1/y\,.\,n\,.\,h)(1/Z^*(f))$, measurements were carried out using a 1260 Solartron Frequency Response Analyser in the 1 Hz to 2 MHz frequency (f) range and voltage amplitude equal to 100 mV in 200–325 K temperature range. Fig. 1d shows the picture of the polymer system used to carry out the electrical measurements.

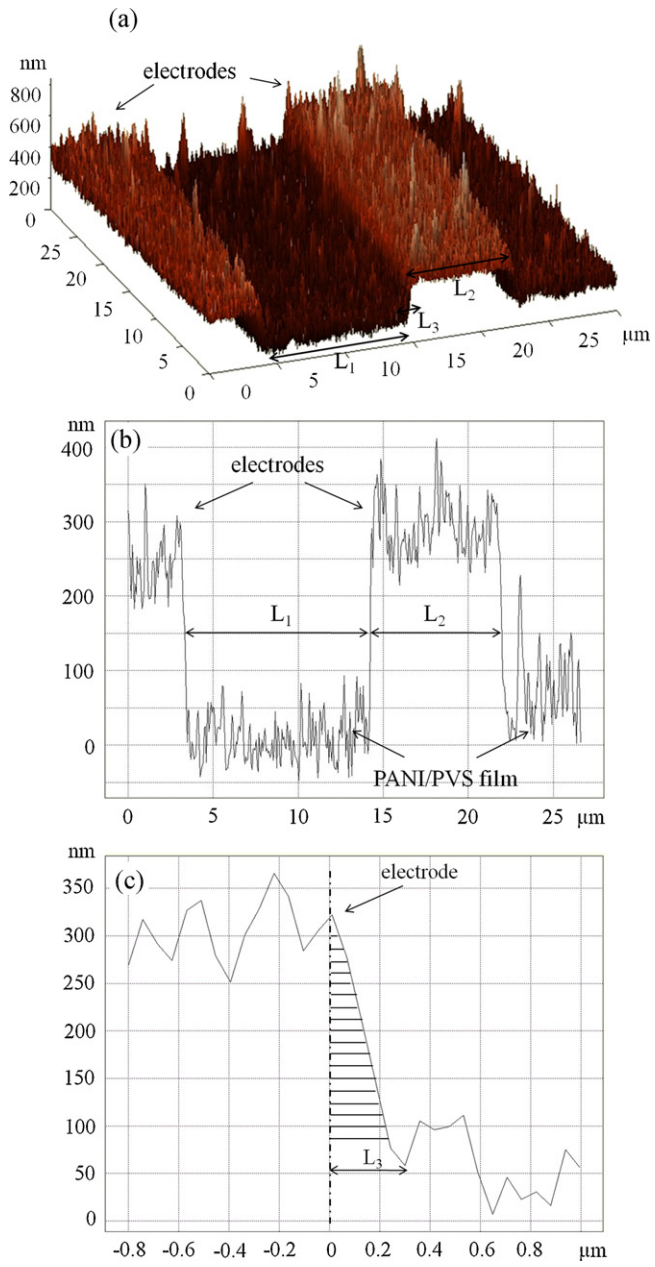

Fig. 2. Images of atomic force microscopy (AFM) of the interdigitated microelectrodes covered with PANI/PVS system, where L_1, L_2 and L_3 correspond to the interdigitated spacing, microelectrodes width and the edges between the metallic electrode and PANI/PVS film surface, respectively. (a) The superficial structure of the interdigitated microelectrodes with 13 bilayers of PANI/PVS system. Panel (b) and (c) show the sidewall profile of the metallic electrode and PANI/PVS regions represented by hatched area.

3. Results and discussion

In order to confirm the dimensions of the microelectrode array provided by the manufacturer, Fig. 2 shows AFM images of the interdigitated microelectrodes covered with PANI/PVS system, where L_1, L_2 and L_3 correspond to the interdigitated spacing, microelectrodes width and the edges between the metallic electrode and PANI/PVS film surface, respectively. Fig. 2a shows the superficial topography of the interdigitated microelectrodes with 13 bilayers of PANI/PVS system, while Fig. 2b and c shows the sidewall profile of the metallic electrode and PANI/PVS regions. Moreover, the sidewall profile obtained from the AFM images allowed us to observe that $L_3 \sim 0.3$ μm is much smaller than L_1 (10 μm). This value of L_3 is not an image artifact, because the AFM tip employed has a cone side angle of ~20° which can read such step edge angle (~45°) of the sample without touching the tip side. It is worth noting that this result is important to propose herein a realistic and ideal parallel plate capacitor structure to study the electrical response of NiCr/Au–PANI/PVS–NiCr/Au structure.

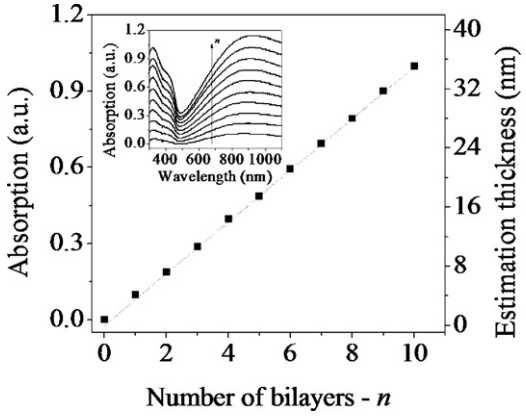

Fig. 3. Absorption at 900 nm and estimated thickness according to the number of bilayers (n). The inset shows the UV–vis absorption spectra for PANI/PVS Lbl system with n varying from 1 to 10.

Fig. 3 shows the absorption and the estimated thickness of the polymer films according to the number of bilayers (n). The linear increase at the maximum absorption (ca. 900 nm) with n indicates that the same amount of material was probably adsorbed in each deposition step. The inset in Fig. 3 shows the UV–vis absorption spectra for PANI/PVS Lbl system with n varying from 1 to 10. It is observed an absorption band at ca. 900 nm, which is characteristic of PANI doped state, while the estimated thicknesses of a multilayer films (from $n = 1$ to 10) were obtained from measuring the thickness of the film with 40 bilayers (see Section 2) and the extrapolation of the linear dependence of the absorption curve as shown in Fig. 3. The value of a single bilayer around 3.5 nm is in agreement with literature for other semiconducting polymers Lbl films [26].

Fig. 4 shows the electrical resistance (R_0) vs. number of PANI/PVS bilayers (n) obtained from NiCr/Au–PANI/PVS–NiCr/Au structure. The R_0 values were obtained from current vs. voltage curves which presented a perfect ohmic and symmetric behavior for forward and reverse bias modes, as shown in inset in Fig. 4. It is observed that R_0 has its value changed drastically and abruptly when the thickness of the films reached the Au contact or was nearly the NiCr layer

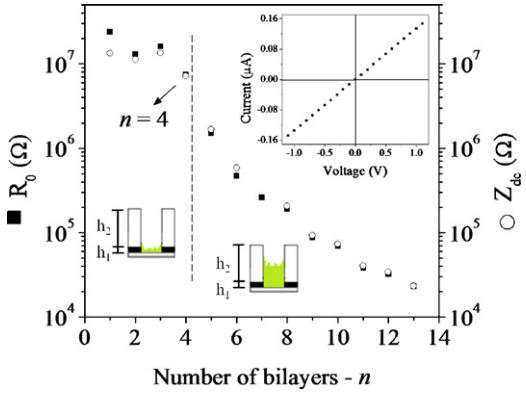

Fig. 4. Electrical resistance (R_0) and real component of the complex impedance at low frequencies (Z_{dc}) vs. number of PANI/PVS bilayers (n). The inset shows the I vs. V measurements obtained with a PANI/PVS Lbl film ($n = 13$) and the schematic illustration of one pair of the interdigitated microelectrodes covered with PANI/PVS system, where h_1 and h_2 correspond to NiCr and Au layer thicknesses, respectively.

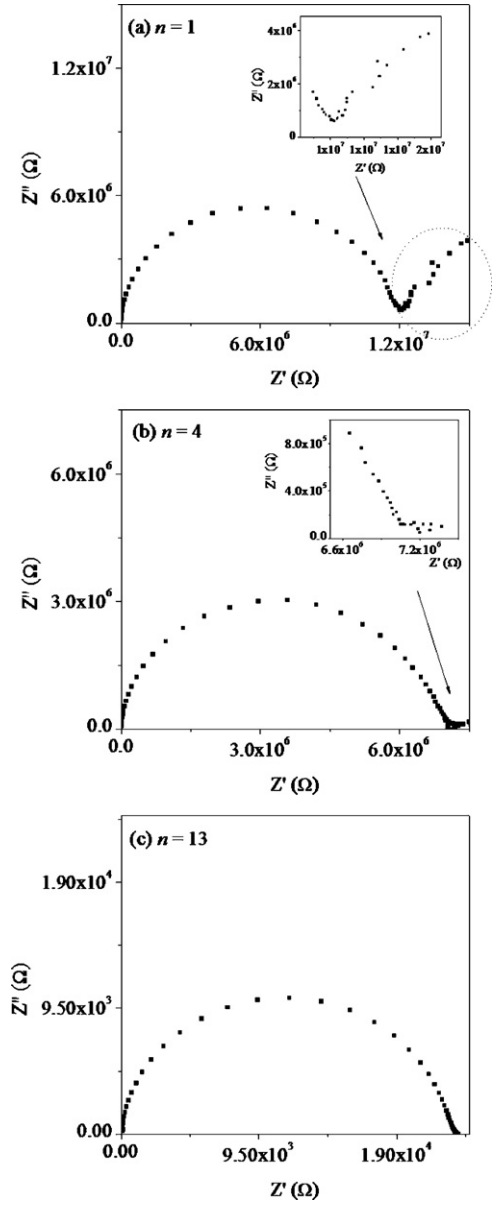

Fig. 5. Argand complex plane obtained from samples with (a) 1, (b) 4 and (c) 13 bilayers.

(h_1 = 20 nm), i.e., n = 5, in such a way that R_0 remains almost constant for $n \leq 4$ and decreased as the number of bilayers increases for $n \geq 5$. This effect was attributed to the higher electrical resistance between the NiCr layer and the PANI/PVS system, in comparison to the Au layer, exhibiting a resistance in the range from $7 \times 10^7\ \Omega$ (n = 1) to $1 \times 10^4\ \Omega$ (n = 13).

Fig. 4 also shows the real component of the complex impedance of NiCr/Au–PANI/PVS–NiCr/Au structure at low frequencies, $Z_{dc} = Z^*(f \rightarrow 0)$, as function of n. Again, R_0 and thus Z_{dc} remains almost constant for $n \leq 4$ and decrease for $n \geq 5$. The inset in Fig. 4 also shows the schematic illustration of a pair of microelectrodes covered with PANI/PVS system for $n \leq 4$ and $n \geq 5$, where h_1 and h_2 correspond to NiCr and Au layer thicknesses, respectively.

Fig. 5 shows the Argand complex plane obtained from NiCr/Au–PANI/PVS–NiCr/Au structure with n equal to 1, 4 and 13. All curves show a semicircle at low real impedance values while a second semicircle is observed only for n = 1, as outlined in the inset of Fig. 5a, where the electrode effect on the electrical response of the system is more pronounced. Fig. 5b and c shows a single semicircle

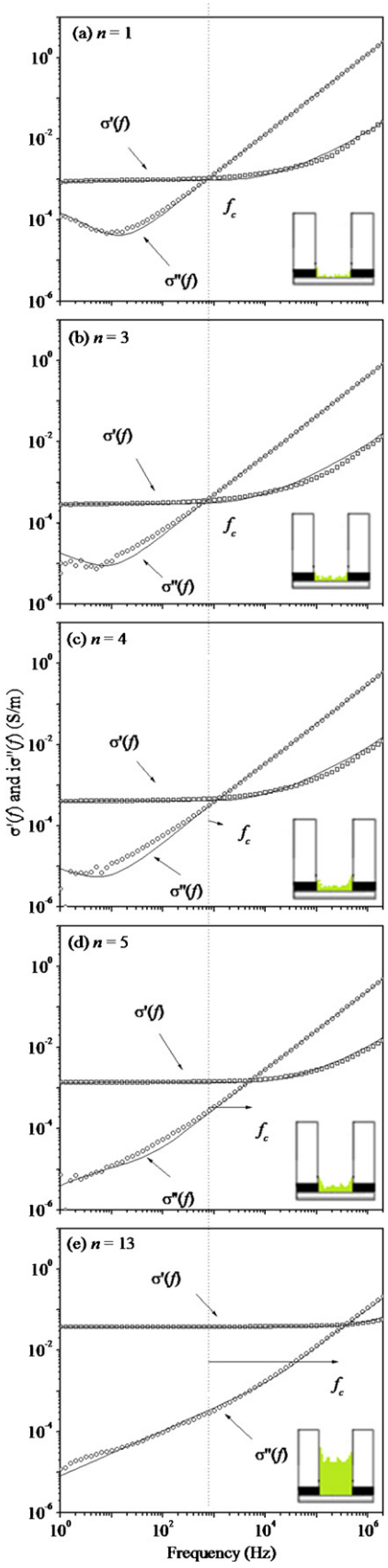

Fig. 6. Real σ' (f) and imaginary σ'' (f) components of ac conductivity as a function of the frequency (f) obtained from samples with (a) n = 1, (b) n = 3, (c) n = 4, (d) n = 5 and (e) n = 13. The inset shows the schematic illustration of a pair of microelectrodes covered with PANI/PVS films for different thickness. The full lines represent the theoretical fitting.

indicating that only one transport mechanism takes place or, at least, dominates the transport process, defining an impedance processes most probably associated to the disordered bulk conduction for $n \geq 5$. It is represented by a unique relaxation time distribution [27]. Moreover, at low frequencies, the value obtained from Z' is similar to R_0, obtained from current vs. voltage curve.

Fig. 6 shows the real $\sigma'(f)$ and imaginary $\sigma''(f)$ components of ac conductivity of NiCr/Au–PANI/PVS–NiCr/Au structure as a function of the frequency (f) obtained from samples with $n = 1$, 3, 4, 5 and 13. From the electrical results showed in this figure, it is observed that at low frequencies the real component increased with n and exhibits a plateau at certain frequency. This frequency, denominated here as the critical frequency, f_c, also increased abruptly from 800 Hz for $n = 1$ to about 400 kHz for $n = 13$. Both $\sigma'(f)$ and $\sigma''(f)$ presented a typical electrode influence at low frequencies (<10 Hz) and bulk effects at higher frequencies. However, this effect is more pronounced in $\sigma''(f)$ at low frequencies. This is consistent with the results shown in Argand complex plane (Fig. 5) and also to the complex impedance measurements of ultrathin PANI films recently carried out in our previous work [28]. Upon increasing the frequency, $\sigma'(f)$ displayed a strong frequency-dependence, obeying the power-law $\sigma'(f) \propto f^s$ ($0 \leq s \leq 1$). This is the typical behavior expected for disordered materials, in which the loss mechanisms present a wide range of possible relaxation times [15,21]. The inset in Fig. 6 shows a schematic illustration of a microelectrode covered with PANI/PVS films for different thickness.

Fig. 7 shows the real $\sigma'(f)$ and imaginary $\sigma''(f)$ components of ac conductivity as a function of the frequency (f) obtained from sample with $n = 13$ for different temperatures. In this case, it was pointed out, in connection with Figs. 4 and 5 that the contribution to $\sigma'(f)$ and $\sigma''(f)$ are related to bulk properties of PANI/PVS system. The same way that the $\sigma'(f)$ for samples with various n, at low frequencies, we have observed that the real component increases with temperature and exhibits a plateau up to critical frequency, while the imaginary component $\sigma''(f)$ irrespectively of the temperature, obeys approximately a linear function in the double logarithm $\sigma''(f) - f$ plot. The Kramers–Krönig relations [29], in the frequency range covered by the present experiments, do not fully determine $\sigma''(f)$ from the knowledge of $\sigma'(f)$, and vice versa. In short, this is because Kramers–Krönig relations are integral (nonlocal) and different behavior obtained for different parameters outside the measured frequency range of the real (imaginary) part influences the behavior of the imaginary (real) part inside the frequency interval. The related problem of inferring the imaginary part from the measured real part was already discussed in the literature [17,30].

The effect of the temperature on $\sigma'(f)$ is displayed in Fig. 8a, for thicker sample ($n = 13$). This figure shows the strong change of $\sigma'(f)$ with temperature when $f < f_c$ and do not display a temperature-dependence for $f > f_c$. We believe that the electronic conduction is via hopping mechanism or phonon assisted tunneling process among localized sites, whose transition rate depends on the spatial distance on the energy difference between two localized sites as described in Ref [18]. It can be observed that the effect of the temperature (in the range of 200–325 K) is similar to that of increase of number of bilayers since the dc conductivity increases with the temperature, as it does with n (Fig. 6). The f_c varies from approximately 3 kHz at 200 K to about 20 kHz at 325 K. The dc conductivity is less than 5×10^{-4} (S/m) at 200 K and ca. 3×10^{-3} (S/m) at 325 K. The relation $\sigma'(f) \propto f^s$ holds above f_c and s seems to be temperature independent ($s \cong 0.7$). A master curve, shown in Fig. 8b, was obtained by plotting the results of Fig. 8a using normalized scales $\sigma'(f)/\sigma_{dc}$ and $f/(Tf_c\sigma_{dc})$. From Figs. 6 and 8, it is also important to remark that the values of $\sigma'(f)$ for $n = 13$ are not the same at 300 K (room temperature) because these measurements were taken under vacuum.

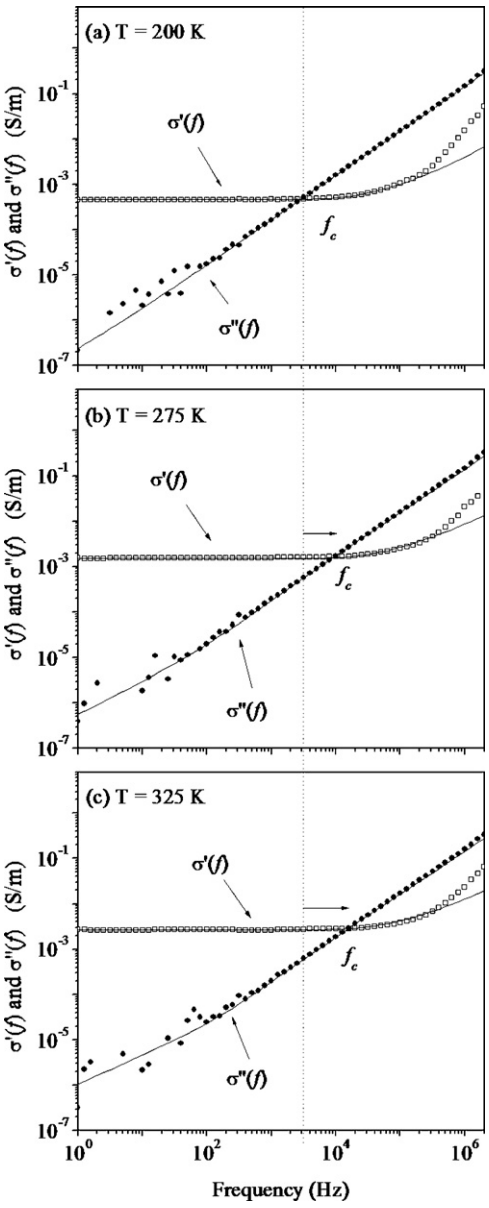

Fig. 7. Real $\sigma'(f)$ and imaginary $\sigma''(f)$ components of ac conductivity as a function of the frequency (f) obtained from sample with $n = 13$ for different temperature under vacuum. The full lines represent the theoretical fittings.

4. Theoretical considerations and fittings

Dyre has proposed the random free energy barrier model (RFEB) for explaining conduction in disordered systems. According to this model, the hopping carrier has to overcome energy barriers randomly distributed between a minimum W_{min} and a maximum energy W_{max} uniformly dispersed through the sample bulk. For low frequencies the thermalized particle has enough time to meet high-energy barriers and the lowest jumping frequency ($\gamma_{min} 2\pi f_c$) [21,22] dominates the process, with $\gamma_{min} = \gamma_0 e^{(-W_{max}/kT)}$, where k is the Boltzmann constant and T is the absolute temperature. This gives rise to the low frequency plateau region. For an electronic hopping process γ_0 depends exponentially on the hopping distance, r, between the sites through the overlap integral of the localized wave functions, by $\gamma_0 = \gamma_0' e^{-2\alpha r}$ where γ_0' is the escape frequency and α is the reciprocal of the electron decay distance. From the mean jumping frequency, Dyre's expression [17,22] for the ac conductivity of disordered materials, $\sigma^*(\omega) = \sigma'(\omega) + i\sigma''(\omega)$,

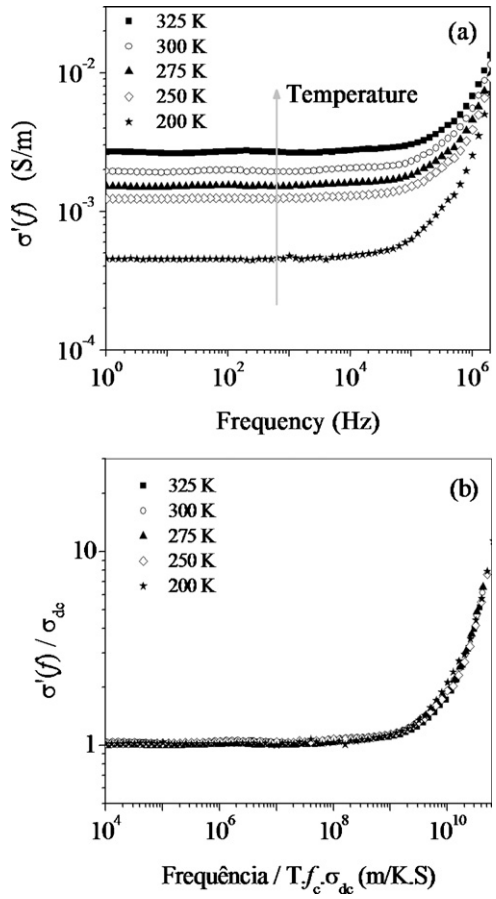

Fig. 8. (a) Real components of the complex conductivity of PANI/PVS system at different temperatures: 200, 250, 275, 300 and 325 K. (b) Master curve obtained from the results of (a) in which each σ' (f) was divided by the correspondent value σ_{dc} and f was divided by ($Tf_c\sigma_{dc}$). All measurements were carried out under vacuum.

is

$$\sigma_D^*(\omega) = \frac{\sigma_0 i\omega/\gamma_{\min}}{\ln(1+(i\omega/\gamma_{\min})/1+(i\omega/\gamma_{\max}))} - \frac{\sigma_0 i\omega}{\gamma_{\min}\ln(\gamma_{\max}/\gamma_{\min})} \quad (1)$$

where $\gamma_{\max} = \gamma_0 e^{(-W_{\min}/kT)}$, ω is the angular frequency ($\omega = 2\pi f$) while σ_0 is the conductivity for $\omega \to 0$, obtained of ac conductivity experimental curves. The real part of Eq. (1) leads to a second high frequency plateau, but if we assume with Dyre that $\gamma_{\max} \gg \gamma_{\min}$, only the one at low frequency will be present, and Eq. (1) is simplified to

$$\sigma_D^*(\omega) = \sigma_0 \left(\frac{i\omega/\gamma_{\min}}{\ln(1+i\omega/\gamma_{\min})} \right) \quad (2)$$

However, the complex conductivity showed in Fig. 6 also shows a capacitive behavior [30]. Thus, the total bulk conductivity must includes the contribution from the dielectric polarization, $\sigma_P^*(\omega)$, which will be written simply as $i\omega\varepsilon'\varepsilon_0$, where ε' is the dielectric constant and ε_0 is the vacuum permittivity. Therefore, the total bulk complex conductivity $\sigma_B^*(\omega)$ is obtained as follows [17,31,32]:

$$\sigma_B^*(\omega) = \sigma_D^*(\omega) + i\omega\varepsilon'\varepsilon_0 \quad (3)$$

Table 1
Data of fittings between Eqs. (4) and (5) and experimental results of ac conductivity for samples with n-bilayers.

n	R_N (MΩ)	C_N (μF)	α_N	σ_{0D} (S/m)	k_P ($\times 10^3$)	$\gamma_{\min}/2\pi$ (Hz)	R_A (kΩ)
1	9.0	0.2	0.8	9.6×10^{-4}	22	3.0×10^3	–
3	3.0	0.6	0.8	3.0×10^{-4}	7.0	1.3×10^3	–
4	0.7	5.0	0.7	4.1×10^{-4}	5.0	2.0×10^3	–
5	0.7	5.0	0.6	1.4×10^{-3}	4.0	8.7×10^3	20
12	0.7	5.0	0.6	3.0×10^{-2}	1.0	2.0×10^5	0.9
13	0.7	5.0	0.6	4.0×10^{-2}	1.0	3.0×10^5	0.6

The carrier transport mechanism in PANI is explained assuming that the sample is considered to be constituted of metallic regions sparsely distributed in a disordered medium, that is, dispersive matrix. It is well known that doped PANI exhibits conductive protonated regions distributed in the bulk of unprotonated matrix. Concerning the disordered matrix we have assumed it to satisfy the RFEB model proposed by Dyre (Eq. (2)) which must included the contribution from polar groups as described in Eq. (3).

Furthermore, the contribution of the interface NiCr–polymer and Au–polymer in the electrical response of the system cannot be neglected. Therefore, based on the configuration of the metal–polymer interface and the polymer bulk, the total complex conductivity of the system is described as two distinct equivalent electrical circuits: one for $n \leq 4$ (Eq. (4)) and other for $n \geq 5$ (Eq. (5)). Eq. (4) represents parallel RC circuits for NiCr–polymer interface and Eq. (3) for polymer properties, while Eq. (5) represents the parallel combinations of RC circuits for NiCr–polymer and Au–polymer interfaces in series with the polymer bulk.

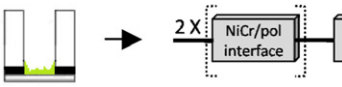

$$\sigma_T^* = \frac{L_1}{A}\left[2.\frac{R_N}{1+(i\omega R_N C_N)\alpha_N} + \frac{L_1}{A}\frac{1}{(\sigma_D^* + i\omega\varepsilon'\varepsilon_0)}\right]^{-1} \quad (4)$$

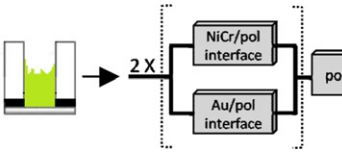

$$\sigma_T^* = \frac{L_1}{A}\left[\frac{2.\frac{R_N}{1+(i\omega R_N C_N)\alpha_N}.2R_A}{2.\frac{R_N}{1+(i\omega R_N C_N)\alpha_N}+2R_A} + \frac{L_1}{A}\frac{1}{(\sigma_D^* + i\omega\varepsilon'\varepsilon_0)}\right]^{-1} \quad (5)$$

R_N, C_N and α_N on Eqs. (4) and (5) correspond to the resistance, capacitance and α parameter of NiCr–PANI/PVS interface, R_A correspond to the resistance of Au–PANI/PVS interface, L_1 is the interdigitated spacing and A is the contact area between the polymer film and the electrodes ($A = ynh$). For NiCr–PANI/PVS interface, which has typically feature insulator, were used the Cole–Cole approach ($\beta = 1$) [33], while for Au–PANI/PVS interface which is ohmic contact (neutral contact), was used a single contact resistance.

Full lines in Figs. 6 and 7 represent the theoretical fitting with the model from this section, in which α_0 estimated from the dc measurements was used as input parameter. The parameters employed are summarized in Tables 1 and 2 for measurements shown in Figs. 6 and 7, respectively.

Table 1 shows the value of parameters R_N, C_N and α_N and R_A related to the interface metal–polymer and σ_0, k_P and $\gamma_{\min}$ related to the bulk response obtained in the fitting of σ' (f) and σ'' (f) for samples with n-bilayers. It is observed that R_N decreases while C_N increases with the contact area (A) of the Lbl films for n varying from

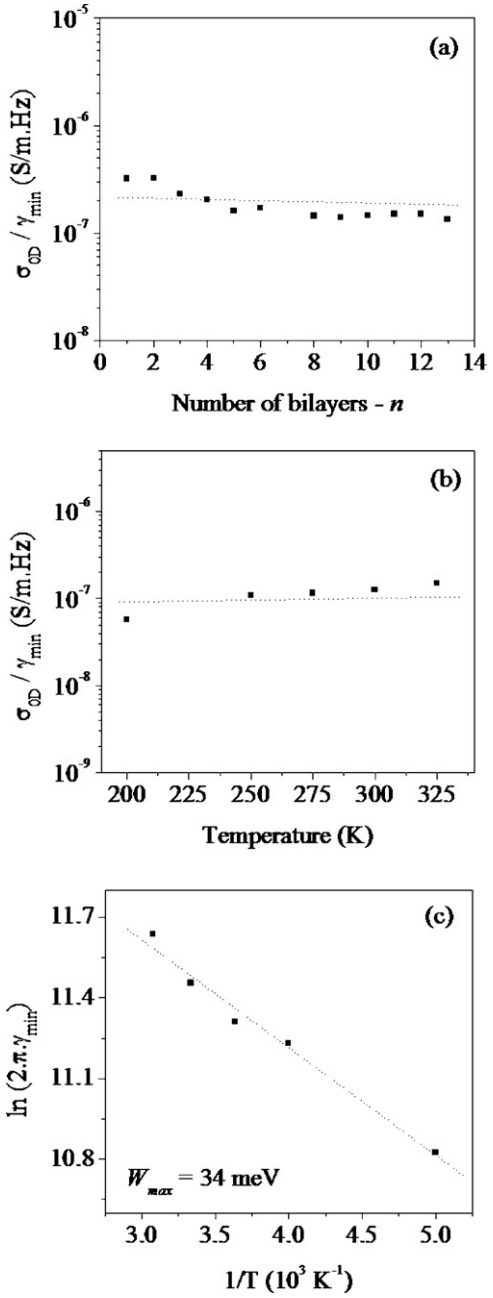

Fig. 9. The ratio σ_0/γ_{min} (a) for samples with n bilayers and (b) for sample with 13 bilayers at different temperature. (c) $\ln(2\pi\gamma_{min})$ vs. T^{-1} from data of Table 2. The curve presents an activation energy $W_{max} = (34 \pm 2)$ MeV when fitted by Arrhenius process. The dot lines are used only to guide the eyes.

1 to 4, reaching constant values for $n \geq 5$. Moreover, the electrical resistance attributed to NiCr–PANI/PVS interface is much higher than the values obtained from the interface Au–PANI/PVS. Furthermore, k_P decreases with n and the obtained values are much higher that the values obtained from PANI films in the literature indicating that some influence of PVS is attributed to PANI/PVS system. This assumption is still under investigation. Finally, the conductivity σ_0 and the γ_{min} increase with the number of bilayers. However, the ratio σ_0/γ_{min} remains almost constant, as shown in Fig. 9a. A similar result was observed when temperature is the experimentally varied parameter, Fig. 9b. This result suggests that the mobility of charge carriers increases with n and T, while the density of these carriers is constant as described for other polyaniline system [17].

Table 2
Data of fittings between Eqs. (4) and (5) and experimental results of ac conductivity for the sample with 13 bilayers at different temperatures.

T (K)	R_N (MΩ)	C_N (μF)	α_N	σ_{0D} (S/m)	k_P ($\times 10^3$)	$\gamma_{min}/2\pi$ (Hz)	R_A (kΩ)
200	0.90	3.0	0.60	4.6×10^{-4}	2.4	8.0×10^3	8.5
250	0.70	5.0	0.60	1.3×10^{-3}	2.2	1.2×10^4	6.0
275	0.50	7.0	0.60	1.5×10^{-3}	2.1	1.3×10^4	4.0
300	0.10	20	0.60	1.9×10^{-3}	2.0	1.5×10^4	1.8
325	0.09	30	0.60	2.7×10^{-3}	2.0	1.8×10^4	1.1

Table 2 shows values of the same set of parameters as in Table 1 obtained from measurements with the 13 bilayers sample for different temperatures from 200 K to 325 K. Again, it is observed that R_N, R_A decrease and C_N increase with the temperature while k_P and α_N remains almost constant. Moreover, both σ_0 and γ_{min} decay exponentially with the temperature, a typical behavior of the Arrhenius process, having the activation energy, $W_{max} = (34 \pm 2)$ MeV, as shown in Fig. 9c. It was obtained from $\ln(2\pi\gamma_{min})$ vs. T^{-1} curves. Indeed, we expected Γ_0 ($=\gamma_0/2\pi$) in $\gamma = \gamma_0 e^{(-W/kT)}$ to obey the relation $\Gamma_0 = \Gamma_0' e^{-2\alpha r}$, where Γ_0' is the escape frequency. Assuming 10^{12} Hz for Γ_0' and 0.25 nm^{-1} for α [34] which is the reciprocal of the electron decay distance, the mean distance r is approximately 30 nm for sample with 13 bilayers.

5. Conclusions

The sidewall profile obtained from the AFM images, allowed us to observe that L_3 (~0.3 μm) is much smaller than L_1 (10 μm) in such way that it was possible to propose a realistic theoretical–experimental model to study the electrical response of NiCr/Au–PANI/PVS–NiCr/Au structure. The more important, unexpected, conclusion of this work is that the presence of NiCr electrode does not favor the electrical current in the NiCr/Au–PANI/PVS–NiCr/Au structure: the interface NiCr–PANI/PVS increases significantly the electrical resistance of the system. This fact, especially in association with the influence of morphology [11], explains why the dc conductivity obtained of NiCr/Au–PANI/PVS–NiCr/Au structure is much lower for films with few bilayers. The global result suggested that the electrical response of organic devices prepared with conjugated polymers on an array of NiCr/Au electrodes is related not only to the bulk properties of conjugated polymers, but also to the interfacial metal–polymer effects and polymer thickness. We believe that our results suggest new directions for the future applications of nanostructured conducting polymer multilayers-based electronic devices in which NiCr provides good adhesion to the glass substrate while Au serves as an ohmic contact.

Acknowledgments

The financial support from MAPA/CNPq (Edital 64/2008), NANOBIOMED/CAPES, INEO/CNPQ (Proc. PDE 200682/2011-2) and FAPEMIG.

References

[1] Y.J. Park, I. Bae, S.J. Kang, J. Chang, C. Park, IEEE Transactions on Dielectrics and Electrical Insulation 17 (2010) 1135–1163.
[2] M.V. Jacob, K. Bazaka, M. Weis, D. Taguchi, T. Manaka, M. Iwamoto, Thin Solid Films 518 (2010) 6123–6129.
[3] A. Riul Jr., R.R. Malmegrim, F.J. Fonseca, L.H.C. Mattoso, Biosensors and Bioelectronics 18 (2003) 1365–1369.
[4] G. Rizzo, A. Arena, N. Donato, M. Latino, G. Saitta, A. Bonavita, G. Neri, Thin Solid Films 518 (2010) 7133–7137.
[5] Kumar Ram Manoj, Yavuz Özlem, Lahsangah Vitawat, Aldiss Matt, CO gas sensing from ultrathin nano-composite conducting polymer film, Sensors and Actuators B 106 (2005) 750–757.
[6] A.T. Royappa, M.F. Rubner, Langmuir 8 (1992) 3168–3177.

[7] J.H. Cheung, W.B. Stockton, M.F. Rubner, Macromolecules 30 (1997) 2712–2716.
[8] G. Machado, M.M. Beppu, A.F. Feil, C.A. Figueroa, R.R.B. Correia, S.R. Teixeira, The Journal of Physical Chemistry C 113 (2009) 19005–19010.
[9] S. Bhadra, D. Khastgir, N.K. Singha, J.H. Lee, Progress in Polymer Science 34 (2009) 783–810.
[10] N.C. Souza, J.R. Silva, R.D. Thommazo, M. Raposo, D.T. Balogh, J.A. Giacometti, O.N. Oliveira Jr., Journal of Physical Chemistry B 108 (2004) 13599–13606.
[11] N.K.L. Wiziack, L.G. Paterno, F.J. Fonseca, L.H.C. Mattoso, Sensors and Actuators B 122 (2007) 484–492.
[12] E.D. Brugnollo, L.G. Paterno, F.L. Leite, F.J. Fonseca, C.J.L. Constantino, P.A. Antunes, L.H.C. Mattoso, Thin Solid Films 516 (2008) 3274–3281.
[13] M.I. Vladu, J.W. Fergus, Synthetic Metals 156 (2006) 1396–1400.
[14] R.F. Bianchi, H.N. da Cunha, R.M. Faria, G.F.L. Ferreira, J.M.G. Neto, Journal of Physics D: Applied Physics 38 (2005) 1437–1443.
[15] T. Cazati, A.C. Maciel, C. Eiras, C.J.L. Constantino, H.N. da Cunha, R.F. Bianchi, Journal of Physics D: Applied Physics 44 (2011) 165301.
[16] G. Machado, A.F. Feil, P. Migowski, L. Rossi, M. Giovanela, J.D. Crespo, L. Miotti, M.A. Sortica, P.L. Grande, M.B. Pereira, R.R.B. Correia, Nanoscale 3 (2011) 1717–1723.
[17] R.F. Bianchi, G.F.L. Ferreira, C.M. Lepienski, R.M. Faria, Journal of Chemical Physics 110 (1999) 4602–4607.
[18] M. Ferreira, A. Riul Jr., K. Wohnrath, F.J. Fonseca, O.N. Oliveira Jr., L.H.C. Mattoso, Analytical Chemistry 75 (2003) 953–955.
[19] D.M. Taylor, A.G. Macdonald, Journal of Physics D: Applied Physics 20 (1987) 1277–1283.
[20] J.R. MacDonald, Journal Applied Physics 62 (1987) R51.
[21] J.C. Dyre, T.B. Schroder, Reviews of Modern Physics 72 (2000) 873–892.
[22] J.C. Dyre, Journal of Applied Physics 64 (1988) 2456–2468.
[23] J.C. Chiang, A.G. MacDiarmid, Synthetic Metals 13 (1986) 193–205.
[24] M. Tominaga, N. Hirata, I. Taniguchi, Electrochemistry Communications 7 (2005) 1423–1428.
[25] K.L. Mittal, Electrocomponent Science and Technology 3 (1976) 21–42.
[26] M. Raposo, R.F.M. Lobo, M.A.P. Da Silva, R.M. Faria, O.N. Oliveira Jr., 10th International Symposium on Electrets, Athens, Greece, 1999.
[27] S. Havriliak, S. Negami, Polymer 8 (1967) 161–210.
[28] M.C. Santos, R.F. Bianchi, 11th International Conference on Advanced Materials, ICAM, Rio de Janeiro, Brazil, 2009.
[29] N.W. Ashcroft, N.D. Mermin, Solid State Physics. Appendix K – Optical Properties of Solids, EUA Cornell University, 1976.
[30] H. Silva, B. Gross, Physical Review 60 (1941) 684.
[31] R.J. Ramos, R.F. Bianchi, D.T. Balogh, R.M. Faria, IEEE Transactions on Dielectrics and Electrical Insulation 7 (2000) 855–859.
[32] R.F. Bianchi, J.A.G. Corrio, S.L. Cuffini, Y.P. Mascarenhas, R.M. Faria, Physical Review B 62 (2000) 10785–10789.
[33] S.C. Raghavendra, S. Khasim, M. Revanasiddappa, M.V.N.A. Prasad, A.B. Kulkarni, Bulletin of Materials Science 26 (2003) 733–739.
[34] P.K. Kahol, V. Pendse, N.J. Pinto, M. Traore, W.T.K. Stevenson, B.J. McCormick, J.N. Gundersen, Physical Review B 50 (1994) 2809.